Chapter 1

Schmidt Magnetic Moments

> *"In the extreme single-particle model the magnetic moment of an odd-A nucleus is attributed to the last unpaired nucleon."*
>
> standard shell-model statement

Lecture 8 treated the deuteron as a two-body magnetic moment. For heavier odd-A nuclei the extreme shell model makes a parallel claim: paired nucleons cancel, and μ is that of the valence nucleon in orbit $n\ell_j$. Plotting the resulting $\mu(j)$ gives the **Schmidt lines** [6, 1, 2].

1.1 Even–even nuclei: vanishing moment

In an even–even ground state every nucleon is paired to $I = 0$. Orbital and spin magnetism cancel within each pair, so

$$\mu = 0 \qquad (I^\pi = 0^+). \tag{1.1}$$

Experiment confirms that even–even ground states carry no static magnetic dipole (consistent with $I = 0$).

1.2 Nuclear magneton and g-factors

Magnetic moments of nuclei are measured in units of the nuclear magneton

$$\mu_N = \frac{e\hbar}{2m_p} \approx 5.05 \times 10^{-27}\,\mathrm{J\,T^{-1}}, \tag{1.2}$$

about 1/1836 of the Bohr magneton $\mu_B = e\hbar/(2m_e)$ because $m_p \gg m_e$. The z-component of the magnetic-moment operator for a single nucleon is

$$\mu_z = (g_\ell\,\ell_z + g_s\,s_z)\frac{\mu_N}{\hbar}, \tag{1.3}$$

with free-nucleon g-factors

$$\begin{aligned} g_\ell^{(p)} &= 1, \quad g_s^{(p)} = 5.5857, \\ g_\ell^{(n)} &= 0, \quad g_s^{(n)} = -3.8260. \end{aligned} \tag{1.4}$$

A useful way to remember the orbital factors is to begin with the magnetic moment of a particle of charge q and mass m:

$$\boldsymbol{\mu}_\ell = \frac{q}{2m}\,\boldsymbol{\ell} = \frac{q}{e}\frac{m_p}{m}\,\frac{\mu_N}{\hbar}\,\boldsymbol{\ell}. \tag{1.5}$$

For a proton, $q = e$ and $m \simeq m_p$, giving $g_\ell^{(p)} = 1$; for a neutron, $q = 0$, giving $g_\ell^{(n)} = 0$ in the leading free one-body operator. In a nucleus, exchange currents and core polarisation can generate effective orbital contributions, so these are baseline coefficients rather than exact in-medium constants. The spin factors follow from the measured intrinsic moments:

$$\mu_p = g_s^{(p)}\frac{\mu_N}{\hbar}\left(\frac{\hbar}{2}\right) = 2.7928\,\mu_N, \qquad \mu_n = \frac{g_s^{(n)}}{2}\mu_N = -1.9130\,\mu_N. \tag{1.6}$$

A pointlike charged Dirac fermion has $g_s = 2$ at tree level; radiative corrections modify that value. The large anomalous moments of the proton and neutron reflect their quark substructure: the proton (uud) and neutron (udd) carry internal charge currents even though the neutron is neutral overall. The neutron therefore has no orbital g_ℓ from net charge, yet a large spin moment [6, 5].

Because of the strong spin–orbit force, the good single-particle angular momentum is $\boldsymbol{j} = \boldsymbol{\ell}+\boldsymbol{s}$. The spectroscopic moment is the expectation value of μ_z in the stretched state $m_j = j$:

$$\mu = \langle j, m_j = j|\, g_\ell \ell_z + g_s s_z \,|j, m_j = j\rangle \frac{\mu_N}{\hbar}. \tag{1.7}$$

1.3 Case $j = \ell + \frac{1}{2}$: unique m_ℓ, m_s

For $j = \ell + \frac{1}{2}$ and $m_j = j = \ell + \frac{1}{2}$, the only combination consistent with $m_\ell + m_s = m_j$ is

$$m_\ell = \ell, \qquad m_s = +\tfrac{1}{2}. \tag{1.8}$$

The coupled state is therefore a single uncoupled basis vector,

$$|j = \ell + \tfrac{1}{2}, m_j = j\rangle = |\ell, m_\ell = \ell\rangle|\tfrac{1}{2}, m_s = \tfrac{1}{2}\rangle. \tag{1.9}$$

Consequently

$$\langle \ell_z\rangle = \ell\hbar, \qquad \langle s_z\rangle = \tfrac{1}{2}\hbar, \tag{1.10}$$

$$\begin{aligned} \frac{\mu}{\mu_N} &= \frac{1}{\hbar}\left(g_\ell \ell\hbar + g_s\frac{\hbar}{2}\right) \\ &= g_\ell \ell + \tfrac{1}{2}g_s. \end{aligned} \tag{1.11}$$

Using $\ell = j - \frac{1}{2}$ gives, one algebraic step at a time,

$$\frac{\mu}{\mu_N} = g_\ell\left(j - \tfrac{1}{2}\right) + \tfrac{1}{2}g_s = j\,g_\ell + \tfrac{1}{2}(g_s - g_\ell). \tag{1.12}$$

Specialising to free g-factors gives the first Schmidt formula

$$\frac{\mu}{\mu_N} = \begin{cases} j + 2.293 & \text{odd proton } (g_\ell = 1,\ g_s = 5.586), \\ -1.913 & \text{odd neutron } (g_\ell = 0,\ g_s = -3.826). \end{cases} \tag{1.13}$$

For a $d_{5/2}$ proton ($\ell = 2$, $j = \frac{5}{2}$), $\mu \approx 4.79\,\mu_N$ on the Schmidt line. For any odd neutron with $j = \ell + \frac{1}{2}$, the Schmidt value equals the free neutron's intrinsic moment, $-1.913\,\mu_N = g_s^{(n)}\mu_N/2$, independent of j, because the leading orbital term vanishes.

1.4 Case $j = \ell - \frac{1}{2}$: two mixed components

For $j = \ell - \frac{1}{2}$ and $m_j = j$, two (m_ℓ, m_s) pairs contribute:

$$\begin{aligned} |1\rangle &= |m_\ell = \ell,\ m_s = -\tfrac{1}{2}\rangle, \\ |2\rangle &= |m_\ell = \ell - 1,\ m_s = +\tfrac{1}{2}\rangle. \end{aligned} \tag{1.14}$$

The stretched state is the normalised combination

$$|j, m_j = j\rangle = a|1\rangle + b|2\rangle. \tag{1.15}$$

1.4.1 Coefficients from $J_+|j, j\rangle = 0$

The raising operator $J_+ = L_+ + S_+$ annihilates the highest-weight state. The two ladder operators act according to

$$L_+|\ell, m_\ell\rangle = \hbar\sqrt{\ell(\ell+1) - m_\ell(m_\ell+1)}\,|\ell, m_\ell + 1\rangle, \tag{1.16}$$

$$S_+|\tfrac{1}{2}, m_s\rangle = \hbar\sqrt{\tfrac{1}{2}(\tfrac{1}{2}+1) - m_s(m_s+1)}\,|\tfrac{1}{2}, m_s + 1\rangle. \tag{1.17}$$

Therefore

$$J_+|1\rangle = (L_+ + S_+)|\ell, -\tfrac{1}{2}\rangle = \hbar|\ell, +\tfrac{1}{2}\rangle, \tag{1.18}$$

$$J_+|2\rangle = (L_+ + S_+)|\ell - 1, +\tfrac{1}{2}\rangle = \hbar\sqrt{2\ell}\,|\ell, +\tfrac{1}{2}\rangle. \tag{1.19}$$

Here the compact ket on the right denotes $|m_\ell = \ell, m_s = +\frac{1}{2}\rangle$. Acting on the mixture now gives

$$\begin{aligned} 0 &= J_+|j, j\rangle = aJ_+|1\rangle + bJ_+|2\rangle \\ &= \hbar(a + b\sqrt{2\ell})|\ell, +\tfrac{1}{2}\rangle. \end{aligned} \tag{1.20}$$

Since the ket and $\hbar$ are nonzero, the coefficient must vanish:

$$a + b\sqrt{2\ell} = 0 \qquad \Rightarrow \qquad a = -b\sqrt{2\ell}, \tag{1.21}$$

together with normalisation $|a|^2 + |b|^2 = 1$. Therefore

$$|a|^2 = \frac{2\ell}{2\ell + 1}, \qquad |b|^2 = \frac{1}{2\ell + 1}. \tag{1.22}$$

Choosing an irrelevant overall phase so that $b > 0$, the normalized state can be written explicitly as

$$|j = \ell - \tfrac{1}{2}, j\rangle = -\sqrt{\frac{2\ell}{2\ell+1}}\,|1\rangle + \sqrt{\frac{1}{2\ell+1}}\,|2\rangle. \tag{1.23}$$

These are precisely the Clebsch–Gordan coefficients for coupling ℓ and $s = \frac{1}{2}$ to $j = \ell - \frac{1}{2}$.

1.4.2 Expectation value of μ_z

Diagonal matrix elements of the magnetic operator are

$$\begin{aligned}\langle 1|\mu_z/\mu_N|1\rangle &= g_\ell \ell - \tfrac{1}{2} g_s, \\ \langle 2|\mu_z/\mu_N|2\rangle &= g_\ell(\ell - 1) + \tfrac{1}{2} g_s,\end{aligned} \tag{1.24}$$

and cross terms vanish by orthogonality of the $|m_\ell m_s\rangle$ basis. More explicitly, ℓ_z and s_z are diagonal in this basis, so

$$\langle 1|\ell_z|2\rangle = \langle 1|s_z|2\rangle = 0. \tag{1.25}$$

This diagonality, not orthogonality alone for an arbitrary operator, is the reason the interference terms vanish. Expanding the full matrix element,

$$\begin{aligned}\frac{\mu}{\mu_N} &= (a^*\langle 1| + b^*\langle 2|)\frac{g_\ell \ell_z + g_s s_z}{\hbar}(a|1\rangle + b|2\rangle) \\ &= |a|^2\langle 1|\mu_z/\mu_N|1\rangle + |b|^2\langle 2|\mu_z/\mu_N|2\rangle \\ &\quad + a^* b\langle 1|\mu_z/\mu_N|2\rangle + b^* a\langle 2|\mu_z/\mu_N|1\rangle.\end{aligned} \tag{1.26}$$

The last line is zero, and the weighted average is therefore

$$\frac{\mu}{\mu_N} = |a|^2(g_\ell \ell - \tfrac{1}{2} g_s) + |b|^2(g_\ell(\ell - 1) + \tfrac{1}{2} g_s). \tag{1.27}$$

Insert $|a|^2 = 2\ell/(2\ell + 1)$ and $|b|^2 = 1/(2\ell + 1)$:

$$\begin{aligned}\frac{\mu}{\mu_N} &= \frac{2\ell}{2\ell+1}(g_\ell \ell - \tfrac{1}{2} g_s) + \frac{1}{2\ell+1}(g_\ell(\ell - 1) + \tfrac{1}{2} g_s) \\ &= \frac{1}{2\ell+1}\Big[2\ell^2 g_\ell - \ell g_s + (\ell - 1)g_\ell + \tfrac{1}{2} g_s\Big] \\ &= \frac{1}{2\ell+1}\Big[(2\ell^2 + \ell - 1)g_\ell - (\ell - \tfrac{1}{2})g_s\Big].\end{aligned} \tag{1.28}$$

Now set $j = \ell - \frac{1}{2}$, so $\ell = j + \frac{1}{2}$ and $2\ell + 1 = 2j + 2$. The two coefficients in the numerator become

$$2\ell^2 + \ell - 1 = 2(j + \tfrac{1}{2})^2 + (j + \tfrac{1}{2}) - 1 = 2j^2 + 3j = j(2j + 3), \tag{1.29}$$

$$\ell - \tfrac{1}{2} = j. \tag{1.30}$$

Thus

$$\frac{\mu}{\mu_N} = \frac{j(2j+3)g_\ell - jg_s}{2(j+1)}$$
$$= \frac{j}{2(j+1)}\left[(2j+3)g_\ell - g_s\right]. \tag{1.31}$$

Adding and subtracting $jg_\ell/[2(j+1)]$ in the last expression gives the equivalent standard Schmidt form

$$\frac{\mu}{\mu_N} = \frac{j}{2(j+1)}\left[(2j+3)g_\ell - g_s\right] = j\,g_\ell - \frac{j}{2(j+1)}(g_s - g_\ell). \tag{1.32}$$

Specialising to free g-factors:

$$\frac{\mu}{\mu_N} = \begin{cases} \dfrac{j}{j+1}\,(j - \tfrac{1}{2}g_s^{(p)} + \tfrac{3}{2}) = \dfrac{j(j-1.293)}{j+1} & \text{odd proton,} \\ -\dfrac{j}{2(j+1)}\,g_s^{(n)} = +1.913\,\dfrac{j}{j+1} & \text{odd neutron.} \end{cases} \tag{1.33}$$

For an odd neutron in $p_{1/2}$ ($j = \frac{1}{2}$), $\mu/\mu_N = 1.913 \times \frac{1}{2}/\frac{3}{2} = 0.638$. These limiting curves are the Schmidt lines first discussed by Schmidt in 1937 [18, 6, 1].

1.4.3 Independent check: the projection theorem

The same result follows without writing Clebsch–Gordan coefficients. Rotational symmetry requires the expectation value of any vector operator in $|jm_j\rangle$ to point along $\boldsymbol{j}$. Hence

$$\langle \ell_z \rangle = \frac{\langle \boldsymbol{\ell}\cdot\boldsymbol{j}\rangle}{j(j+1)\hbar^2}\,m_j\hbar, \qquad \langle s_z \rangle = \frac{\langle \boldsymbol{s}\cdot\boldsymbol{j}\rangle}{j(j+1)\hbar^2}\,m_j\hbar. \tag{1.34}$$

Using $\boldsymbol{j} = \boldsymbol{\ell} + \boldsymbol{s}$,

$$2\boldsymbol{\ell}\cdot\boldsymbol{j} = \boldsymbol{j}^2 + \boldsymbol{\ell}^2 - \boldsymbol{s}^2, \tag{1.35}$$
$$2\boldsymbol{s}\cdot\boldsymbol{j} = \boldsymbol{j}^2 - \boldsymbol{\ell}^2 + \boldsymbol{s}^2. \tag{1.36}$$

For the spectroscopic state $m_j = j$, division by $\hbar$ gives

$$\frac{\langle \ell_z\rangle}{\hbar} = \frac{j(j+1) + \ell(\ell+1) - s(s+1)}{2(j+1)}, \tag{1.37}$$
$$\frac{\langle s_z\rangle}{\hbar} = \frac{j(j+1) - \ell(\ell+1) + s(s+1)}{2(j+1)}. \tag{1.38}$$

Substitution into $\mu/\mu_N = g_\ell\langle\ell_z\rangle/\hbar + g_s\langle s_z\rangle/\hbar$, with $s = \frac{1}{2}$, reproduces Eqs. (1.13) and (1.32). This is the same projection theorem used for the deuteron in Lecture 8; it is a valuable check because it keeps every orbital and spin term visible.

1.4.4 Why a one-hole state has the same Schmidt value

A filled j subshell has zero total moment because the contributions from m and $-m$ cancel. To construct a hole state with total $M = +j$, remove the particle with $m = -j$. The remaining shell therefore has

$$\mu_{\text{hole}}(M = +j) = 0 - \mu_{\text{particle}}(m = -j) = \mu_{\text{particle}}(m = +j), \tag{1.39}$$

because a vector moment changes sign under $m \to -m$. Thus a particle and a hole in the same j orbit have the same Schmidt moment in the extreme model, even though their many-body occupations are complementary.

1.5 Schmidt lines and experiment

Plotting μ against j for odd-proton nuclei gives two rising lines ($j = \ell \pm \frac{1}{2}$). For odd-neutron nuclei the $j = \ell + \frac{1}{2}$ line is flat at $-1.913\,\mu_N$ and the $j = \ell - \frac{1}{2}$ line is positive and slowly rising. Experimental ground-state moments of odd-A nuclei typically fall *between* the two Schmidt lines for the assigned j (Fig. 1.1) [18, 6, 2, 22]. The Schmidt curves are theoretical single-particle limits, not rigorous mathematical bounds; they organise the data and diagnose configuration purity.

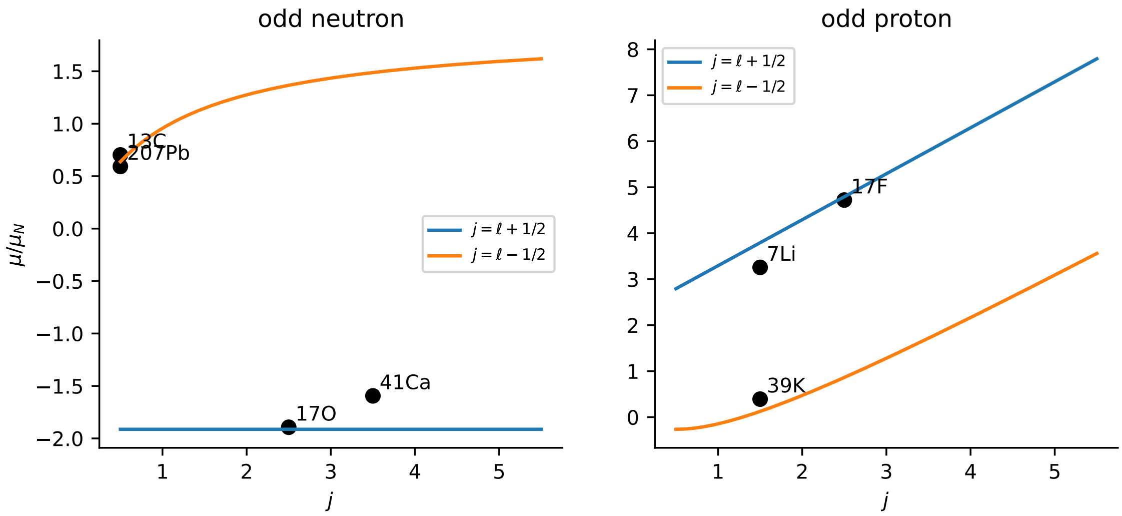

Figure 1.1: Free-nucleon Schmidt curves with selected measured ground-state magnetic moments from the Stone/NNDC compilation (nuclide list and numerical values are recorded in `figures/lecture14/SOURCES.txt`) [22, 20]. Curves are single-particle estimates, not bounds.

1.6 Why real nuclei lie between the Schmidt lines

The extreme single-particle picture is too simple:

- configuration mixing admixes other orbitals with the same I^π;
- meson-exchange currents modify the free one-body magnetic operator inside the nucleus;
- collective core polarisation contributes for soft nuclei far from closed shells;
- restricted shell-model spaces often use effective spin g-factors with $|g_s|$ reduced from the free value. A rough sd- or pf-shell starting estimate is $g_s^{\text{eff}} \sim (0.7\text{–}0.8)g_s^{\text{free}}$, but the factor depends

on model space, interaction, mass region, and operator; it is neither a universal property of nuclear matter nor interchangeable with axial-current quenching in weak transitions [6, 1].

Near doubly magic cores (e.g. ^{17}O, ^{41}Ca) agreement with Schmidt values is better; mid-shell nuclei deviate more [6, 2, 1, 22]. When a measured μ lies close to one Schmidt line, the valence assignment $j = \ell \pm \frac{1}{2}$ is strongly supported; intermediate values tag mixing.

Key idea

Schmidt lines are the shell-model baseline for μ. They fix the single-particle g-factors and $j = \ell \pm \frac{1}{2}$ assignment; deviations measure correlations beyond the extreme model.

1.7 Deeper physics: Schmidt lines, g-factors, and quenching

1.7.1 Schmidt limits as independent-particle bounds

For an odd-A nucleus with one unpaired nucleon in orbit ℓ, the magnetic operator (1.3) evaluated in the stretched state $|j, m = j\rangle$ yields the Schmidt formulae (**??**, **??**). For an unpaired proton,

$$\frac{\mu}{\mu_N} = \begin{cases} j + \frac{1}{2}(g_p - 1) = \ell + 1 + \frac{1}{2}(g_p - 1), & j = \ell + \frac{1}{2}, \\ j - \frac{j}{2(j+1)}(g_p - 1), & j = \ell - \frac{1}{2}, \end{cases} \tag{1.40}$$

with free $g_p = 5.5857$. Real nuclei fall *between* the two curves because core polarisation, configuration mixing, and meson-exchange currents reduce the effective spin response.

1.7.2 Quenching as a compact summary

When a measured moment lies below the upper Schmidt line, one often writes an **effective** spin g-factor $g_s^{\text{eff}} < g_s^{\text{free}}$. This is a phenomenological compression of several mechanisms, not a fundamental constant. Near ^{16}O or ^{40}Ca, odd neighbours such as ^{17}O ($\mu = +1.89\,\mu_N$) sit close to the $d_{5/2}$ Schmidt prediction ($\sim 1.91\,\mu_N$), while mid-shell nuclei can deviate by tens of percent [6, 22].

Schmidt deviation for ^{15}N

^{15}N has an unpaired proton in $1p_{1/2}$ ($I = \frac{1}{2}$). The Schmidt formula with $g_\ell = 1$, $g_s = g_p$, $j = \ell - \frac{1}{2}$ gives $\mu/\mu_N = \frac{1}{2} + \frac{1}{6}(g_p - 1) \approx 0.44$, i.e. $\mu_{\text{Schmidt}} \approx +2.2\,\mu_N$. Experiment gives $\mu = -0.283\,\mu_N$: the hole character and core polarisation reverse and quench the moment. Even near ^{16}O, Schmidt lines are guides, not precision predictions [6, 22].

Remark

Link to electroweak observables. Quenching of spin operators also appears in Gamow–Teller β decay and in neutrinoless double-beta matrix elements. Modern calculations renormalise *both* the Hamiltonian and the operator consistently rather than applying an ad hoc g_A^{eff} after the fact (Lecture 14 further material).

1.7.3 Even–even neighbours as Schmidt context

Schmidt lines apply only to odd-A nuclei. The adjacent even–even core has $\mu = 0$ (Section 1.1), and its first 2^+ energy (Lecture 15) indicates whether the core is rigid (high $E(2^+)$, Schmidt works well) or soft/collective (low $E(2^+)$, Schmidt fails). Plotting μ against $E(2^+)$ of the $A - 1$ neighbour separates closed-shell odd nuclei from mid-shell ones without invoking a full shell-model calculation [6, 22].

1.7.4 Sign of μ and hole vs particle orbits

A valence *proton* and a valence *proton hole* on the same orbit produce opposite Schmidt limits once the hole sign $(-1)^{N_\mathrm{h}}$ is applied. ^{15}N (p hole on ^{16}O) and ^{17}F (p particle, $1d_{5/2}$) illustrate mirror magnetic behaviour tied to the same WS filling diagram (Lecture 13). Confusing particle and hole signs is a common source of error when overlaying measured moments on Schmidt plots [2, 6].

1.7.5 Landé g-factor for odd–even nuclei

When several nucleons are unpaired (odd–odd nuclei), the Landé formula generalises the Schmidt limit. For odd-A nuclei with one valence nucleon, the effective g-factor reduces to the Schmidt value in the stretched state. Measuring μ and I separately determines an empirical g_I, which can be compared with shell-model calculations that include core polarisation. Near closed shells the agreement is often within 10%; mid-shell nuclei require full diagonalisation in a truncated space [6, 22].

Remark

Isoscalar versus spin contributions. Orbital g_ℓ factors are close to bare values; spin g_s factors show larger medium renormalisations. Magnetic moments therefore diagnose spin correlations more sharply than electric quadrupole moments diagnose charge deformation (Lecture 15), although both feel configuration mixing.

A practical student plot: Schmidt lines for odd protons with five measured mid-shell moments overlaid. The pattern of deviations is the entire qualitative message of this chapter.

1.8 Further physics: magnetic moments as configuration tags

Measured magnetic moments are among the most sensitive tests of the valence configuration near closed shells. If μ lies close to one Schmidt line, the extreme single-particle assignment $j = \ell \pm \frac{1}{2}$ is strongly supported. Intermediate values signal configuration mixing or collective admixtures [6, 2, 22].

Effective g_s factors reduced from the free nucleon values are a compact way to summarise medium modifications, but they absorb several distinct mechanisms: core polarisation, meson-exchange currents, and truncated model spaces. For that reason one should not treat a single quenching factor as fundamental. Near doubly magic cores such as ^{16}O and ^{40}Ca, moments of neighbouring odd-A nuclei remain comparatively close to Schmidt predictions; far from magic numbers, collective contributions dominate and the Schmidt picture is only a reference baseline.

1.8.1 Plotting Schmidt lines: odd-proton example

For an unpaired proton, (1.40) gives two curves in the $(I, \mu/\mu_N)$ plane. At $I = \frac{1}{2}$ (from $p_{1/2}$ or $f_{7/2}$), the upper line yields $\mu/\mu_N = 0.44$ and the lower line gives $\mu/\mu_N = -0.25$. At $I = \frac{7}{2}$ (from $f_{7/2}$ aligned), $\mu/\mu_N = 4.71$ (upper) and 3.79 (lower). Measured moments of odd-Z nuclei between $20 \le Z \le 40$ cluster between the curves, with deviations growing toward mid-shell where collective admixtures appear [22, 6].

1.8.2 Quenching: one number, several mechanisms

Writing $\mu_{\text{exp}} = g_s^{\text{eff}} \mu_{\text{Schmidt}}$ compresses:

- **Configuration mixing:** valence spin is shared among several j-shells (Lecture 13).
- **Core polarisation:** paired nucleons are excited by the valence nucleon and contribute opposite magnetism.
- **Meson-exchange currents:** two-body operators (pp, pn currents) add to the one-body Schmidt operator (Lecture 8 further material).

Separating these requires a model, not just a table of moments. The deuteron deficit is the minimal case where only mechanism (iii) and a few-percent D-wave compete [2, 50].

Gamow–Teller quenching scale

Historically, shell-model β decay rates required $g_A^{\text{eff}}/g_A \approx 0.75$. Modern ab initio calculations with two-body currents recover much of that quenching without an ad hoc factor, paralleling the magnetic-moment story. The same operator renormalisation feeds $0\nu\beta\beta$ matrix elements (Lecture 14 research frontier) [50, 49].

1.8.3 Bridge to Lecture 15 spectroscopic factors

A nucleus whose moment lies on a Schmidt line usually has a large spectroscopic factor for adding or removing the valence nucleon (Lecture 15). When both μ and S deviate, configuration mixing is confirmed from two independent probes. Even–even neighbours with low $E(2^+)$ (Lecture 15) signal that the odd-A Schmidt picture is only a local approximation near closed shells [6, 1].

1.8.4 Stone table as experimental anchor

Evaluated magnetic moments (Stone tables) remain the benchmark for shell-model and ab initio calculations. Near ^{16}O and ^{40}Ca, odd neighbours often lie within $\sim 20\%$ of Schmidt lines; in the $A \sim 100$ region deviations exceed 50%, signalling collective admixtures and strong configuration mixing. Any student overlay of Schmidt curves should quote uncertainties on μ and note whether the state is isomeric or ground-state [22, 6, 2].

1.8.5 Core polarisation as a picture for quenching

When a valence nucleon moves, it polarises closed-shell pairs in the core: particle–hole excitations of the core contribute magnetism opposite to the valence spin. In a truncated shell-model space this appears as configuration mixing; in an ab initio calculation it is part of the correlated wave function. Either way, the measured moment lies between the Schmidt lines. The deuteron has no inert core, so its quenching is dominated by D-wave mixing and exchange currents rather than core polarisation, simplifying the interpretation at $A = 2$ [6, 50, 2].

1.9 Deeper reading: g-factors, quenching, and operators

Schmidt lines bound single-particle magnetic moments for odd-A nuclei near closed shells. Mid-shell moments fall inside the lines because of configuration mixing. An effective g_s quenching was long used phenomenologically; modern work attributes much of Gamow–Teller and magnetic quenching to two-body currents treated consistently with correlations, a lesson already previewed in the deuteron (Lecture 8).

For $0\nu\beta\beta$ matrix elements (Lecture 19), the same operator renormalisation issues return at higher stakes: an inconsistent g_A^{eff} stacked on top of an already-renormalised operator double counts physics. Evaluated moment tables remain the benchmark against which both shell-model and ab initio calculations are judged.

Magnetic moments as operator diagnostics

Because magnetic moments weight spin strongly, they expose quenching and meson-exchange currents more clearly than binding energies do. A model that fits spectra with effective charges may still fail moments unless operators are renormalised consistently. Build a habit of checking moments whenever a new effective interaction is proposed.

Mirror magnetic moments

Differences between mirror magnetic moments isolate isovector operator pieces and Coulomb-induced configuration changes. They are a precision testbed complementary to isoscalar deuteron lessons (Lecture 8).

Schmidt diagram exercise

Draw Schmidt lines for odd protons and odd neutrons. Overlay ^{17}F, ^{17}O, a mid-shell odd-A nucleus, and a deformed rare-earth moment. The closed-shell neighbours hug the lines; the mid-shell point falls inside; the deformed example may require collective g_R contributions. Write one sentence for each point naming the dominant physics.

Then estimate a naive quenching factor from one Gamow–Teller $\log ft$ compared with an extreme single-particle matrix element. Discuss why that single number should not be transplanted into a $0\nu\beta\beta$ calculation that already includes two-body currents. The exercise links Lectures 8, 14, and 19 into one operator story.

Schmidt lines are baselines, not predictions for mid-shell nuclei. Deviations teach configuration mixing and operator renormalisation, preparing the weak-interaction chapters.

In practice, rework one numerical estimate from the lecture with a different parameter set and compare the shift to the quoted experimental uncertainty. If the shift exceeds the uncertainty, the estimate is teaching a scale, not delivering a fit. That distinction keeps theoretical cartoons honest when they sit beside evaluated data tables and modern many-body calculations. Along the course arc, write one sentence linking this chapter backward and one forward: the discipline of those two sentences is as important as any single formula. Examination problems rarely ask for a literature review, but they do ask for the scale argument that literature reviews presuppose.

Synthesis problem

Write a half-page note that (i) restates the chapter's central scale or selection rule in one equation, (ii) evaluates it numerically for one concrete nucleus or energy, and (iii) names the neighbouring lecture that uses the result. Keep the note free of research-frontier speculation; the goal is fluency with the lecture physics itself. If an assumption fails (Born approximation, spherical mean field, allowed transition, one-dimensional barrier), state the failure mode in a final sentence. That habit converts passive reading into examination-ready understanding and makes the later research-frontier box read as an extension rather than a replacement.

Research frontier: electroweak operators and student projects

Schmidt lines (Lecture 14) still organise magnetic moments of odd-A nuclei near closed shells, but modern theory computes effective g-factors and Gamow–Teller operators from correlated wave functions and two-body currents. A landmark ab initio study showed that consistent two-body currents resolve much of the long-standing GT quenching, with direct implications for β-decay rates and for neutrinoless double-beta nuclear matrix elements [50, 49]. Evaluated moment tables remain the experimental reference against which shell-model and ab initio calculations are judged [22]. Open questions include how large residual quenching is in heavy nuclei, how operator renormalisation should be matched to the Hamiltonian truncation, and how those lessons propagate into $0\nu\beta\beta$ matrix-element uncertainties that limit neutrino-mass sensitivity claims [48]. Treating Hamiltonian correlations and electroweak operators inconsistently remains a common source of theoretical bias.

A concrete way to see operator renormalisation is to compare a bare GT matrix element in a small valence space with a published calculation that includes two-body currents. The fractional change is often comparable to the historical quenching factor, which is why modern papers discourage applying an extra ad hoc g_A^{eff} on top of already-renormalised operators.

The same consistency requirement appears in calculations of magnetic moments far from Schmidt lines.

Student directions. (1) Data plot: draw Schmidt lines for odd protons and overlay five measured moments. (2) Estimate: extract a single phenomenological quenching factor g_A^{eff}/g_A from one mid-shell GT transition and discuss its limitations. (3) Essay: explain why operator renormalisation and Hamiltonian correlations must be treated consistently for $0\nu\beta\beta$ matrix elements.

1.10 Problems with solutions

Problem 14.1 — Schmidt value for $d_{5/2}$ proton

Compute the Schmidt moment for an odd proton in $j = \ell + \frac{1}{2} = \frac{5}{2}$.

Solution 14.1

For $j = \ell + \frac{1}{2}$ and free proton g-factors,

$$\frac{\mu}{\mu_N} = j\, g_\ell + \tfrac{1}{2}(g_s - g_\ell) = \tfrac{5}{2} \cdot 1 + \tfrac{1}{2}(5.586 - 1) = 2.5 + 2.293 = 4.793.$$

Equivalently, $\mu/\mu_N = j + 2.293$ [18, 6].

Problem 14.2 — Neutron $p_{1/2}$ Schmidt moment

For an odd neutron with $j = \ell - \frac{1}{2} = \frac{1}{2}$ ($\ell = 1$), compute the Schmidt moment in nuclear magnetons.

Solution 14.2

For an odd neutron with $j = \ell - \frac{1}{2}$,

$$\frac{\mu}{\mu_N} = +1.913\, \frac{j}{j+1} = 1.913 \times \frac{1/2}{3/2} = \frac{1.913}{3} \approx 0.638.$$

Equivalently, $\mu/\mu_N = -g_s^{(n)} j/(2(j+1))$ with $g_s^{(n)} = -3.826$ yields the same result [6, 18].

Problem 14.3 — Neutron $j = \ell + \frac{1}{2}$

Show that any odd neutron with $j = \ell + \frac{1}{2}$ has Schmidt moment $\mu = -1.913\, \mu_N$, independent of j.

Solution 14.3

With $g_\ell^{(n)} = 0$ and $g_s^{(n)} = -3.826$, the $j = \ell + \frac{1}{2}$ formula collapses to

$$\frac{\mu}{\mu_N} = \tfrac{1}{2} g_s = -1.913,$$

for every such orbit. Only the spin moment contributes [6, 1].

Problem 14.4 — Coefficients a and b

For $j = \ell - \frac{1}{2}$ and $m_j = j$, derive $|a|^2 = 2\ell/(2\ell + 1)$ and $|b|^2 = 1/(2\ell + 1)$ from $J_+|j, j\rangle = 0$.

Solution 14.4

Write $|j, j\rangle = a|1\rangle + b|2\rangle$ with $|1\rangle = |\ell, -\frac{1}{2}\rangle$ and $|2\rangle = |\ell - 1, +\frac{1}{2}\rangle$. Acting with $J_+ = L_+ + S_+$ and using $L_+|\ell, m\rangle = \hbar\sqrt{\ell(\ell+1) - m(m+1)}\,|\ell, m+1\rangle$ gives the condition $a + b\sqrt{2\ell} = 0$. Together with $|a|^2 + |b|^2 = 1$ one obtains

$$|a|^2 = \frac{2\ell}{2\ell+1}, \qquad |b|^2 = \frac{1}{2\ell+1},$$

as in the main text [6].

Bibliography

[1] R. A. Dunlap, *An Introduction to the Physics of Nuclei and Particles* (2nd ed.), IOP Publishing, Bristol (2023), DOI: 10.1088/978-0-7503-6094-4, Ch. 3 (Nuclear composition and size).

[2] W. Demtröder, *Nuclear and Particle Physics*, Undergraduate Lecture Notes in Physics, Springer, Cham (2023).

[3] S. Petrera, *Problems and Solutions in Nuclear and Particle Physics*, UNITEXT for Physics, Springer, Cham (2019).

[4] F. Terranova, *A Modern Primer in Particle and Nuclear Physics*, Oxford University Press (2021).

[5] S. D'Auria, *Introduction to Nuclear and Particle Physics*, Undergraduate Lecture Notes in Physics, Springer, Cham (2018).

[6] K. S. Krane, *Introductory Nuclear Physics*, Wiley, New York (1988).

[7] R. Hofstadter, "Electron scattering and nuclear structure," Rev. Mod. Phys. **28**, 214 (1956).

[8] H. F. Ehrenberg, R. Hofstadter, U. Meyer-Berkhout, D. G. Ravenhall, and S. E. Sobottka, "High-Energy Electron Scattering and the Charge Distribution of Carbon-12 and Oxygen-16," Phys. Rev. **113**, 666 (1959).

[9] H. Yukawa, "On the interaction of elementary particles. I," Proc. Phys.-Math. Soc. Japan **17**, 48 (1935).

[10] R. D. Woods and D. S. Saxon, "Diffuse surface optical model for nucleon-nuclei scattering," Phys. Rev. **95**, 577 (1954).

[11] H. G. J. Moseley, "The high-frequency spectra of the elements," Phil. Mag. **26**, 1024 (1913); **27**, 703 (1914).

[12] C. F. von Weizsäcker, "Zur Theorie der Kernmassen," Z. Phys. **96**, 431 (1935).

[13] P. Cappellaro, *Introduction to Applied Nuclear Physics* (MIT OpenCourseWare / LibreTexts), CC BY-NC-SA 4.0.

[14] J.-L. Basdevant, J. Rich, and M. Spiro, *Fundamentals in Nuclear Physics: From Nuclear Structure to Cosmology*, Springer, New York (2005).

[15] D. Tong, *Particle Physics*, Lecture notes (University of Cambridge / CERN school notes).

[16] M. G. Mayer, "On closed shells in nuclei. II," Phys. Rev. **75**, 1969 (1949).

[17] O. Haxel, J. H. D. Jensen, and H. E. Suess, "On the "magic numbers" in nuclear structure," Phys. Rev. **75**, 1766 (1949).

[18] T. Schmidt, "Über die magnetischen Momente der Atomkerne," Z. Phys. **106**, 358 (1937).

[19] L. W. Nordheim, "On spins, moments, and shells in nuclei," Phys. Rev. **78**, 294 (1950).

[20] Evaluated Nuclear Structure Data File (ENSDF), National Nuclear Data Center, Brookhaven National Laboratory, `https://www.nndc.bnl.gov/ensdf/`.

[21] NuDat 3, National Nuclear Data Center, Brookhaven National Laboratory, `https://www.nndc.bnl.gov/nudat3/`.

[22] N. J. Stone, "Table of nuclear magnetic dipole and electric quadrupole moments," At. Data Nucl. Data Tables **90**, 75 (2005); updated compilations at NNDC.

[23] W. N. Cottingham and D. A. Greenwood, *An Introduction to Nuclear Physics* (2nd ed.), Cambridge University Press, Cambridge (2001).

[24] H. Geiger and J. M. Nuttall, "The ranges of the α particles from the radioactive substances," Phil. Mag. **22**, 613 (1911).

[25] G. Gamow, "Zur Quantentheorie des Atomkernes," Z. Phys. **51**, 204 (1928).

[26] R. W. Gurney and E. U. Condon, "Wave mechanics and radioactive disintegration," Nature **122**, 439 (1928); Phys. Rev. **33**, 127 (1929).

[27] M. Wang, W. J. Huang, F. G. Kondev, G. Audi, and S. Naimi, "The AME 2020 atomic mass evaluation (II). Tables, graphs and references," Chin. Phys. C **45**, 030003 (2021).

[28] Laboratoire National Henri Becquerel (LNHB), Recommended decay data, `http://www.lnhb.fr/nuclear-data/nuclear-data-table/`.

[29] L. M. Langer, R. D. Moffat, and H. C. Price, Jr., "Low energy beta-ray spectra: P^{32} and Cu^{64}," Phys. Rev. **76**, 1725 (1949).

[30] L. M. Langer and H. C. Price, Jr., "Shapes of the beta-spectra of the forbidden transitions of Sb^{124}, Rb^{86}, Sr^{89}, Y^{91}, and Cs^{137}," Phys. Rev. **75**, 1769 (1949).

[31] D. C. Camp and L. M. Langer, "The shape of the ^{66}Ga positron spectrum and the contribution from $0^+ \to 0^+$ transitions," Phys. Rev. **129**, 1782 (1963).

[32] H. C. Verma, *Nuclear Physics: Fundamentals and Applications*, NPTEL/IIT Kanpur lecture series, `https://hcverma.in/ncl_phy_lectures`.

[33] International Atomic Energy Agency, *LiveChart of Nuclides*, evaluated structure, decay, reaction, and fission-yield data, `https://www-nds.iaea.org/relnsd/vcharthtml/VChartHTML.html`.

[34] T. Kibédi, T. W. Burrows, M. B. Trzhaskovskaya, P. M. Davidson, and C. W. Nestor, Jr., "Evaluation of theoretical conversion coefficients using BrIcc," Nucl. Instrum. Methods Phys. Res. A **589**, 202 (2008), DOI: 10.1016/j.nima.2008.02.051.

[35] D. A. Brown *et al.*, "ENDF/B-VIII.0: The 8th major release of the nuclear reaction data library with CIELO-project cross sections, new standards and thermal scattering data," Nucl. Data Sheets **148**, 1 (2018), DOI: 10.1016/j.nds.2018.02.001.

[36] B. Acharya *et al.*, "Solar fusion III: New data and theory for hydrogen-burning stars," Rev. Mod. Phys. **97**, 035002 (2025), DOI: 10.1103/8lm7-gs18.

[37] S. N. Ghoshal, "An experimental verification of the theory of compound nucleus," Phys. Rev. **80**, 939 (1950), DOI: 10.1103/PhysRev.80.939.

[38] D. Adhikari *et al.* (PREX Collaboration), "Accurate determination of the neutron skin thickness of ^{208}Pb through parity-violation in electron scattering," Phys. Rev. Lett. **126**, 172502 (2021), DOI: 10.1103/PhysRevLett.126.172502.

[39] B. T. Reed, F. J. Fattoyev, C. J. Horowitz, and J. Piekarewicz, "Implications of PREX-II on the equation of state of neutron-rich matter," Phys. Rev. Lett. **126**, 172503 (2021), DOI: 10.1103/PhysRevLett.126.172503.

[40] B. Hu *et al.*, "Ab initio predictions link the neutron skin of ^{208}Pb to nuclear forces," Nature Phys. **18**, 1196 (2022), DOI: 10.1038/s41567-022-01715-8.

[41] E. Epelbaum, H.-W. Hammer, and U.-G. Meißner, "Modern theory of nuclear forces," Rev. Mod. Phys. **81**, 1773 (2009), DOI: 10.1103/RevModPhys.81.1773.

[42] H.-W. Hammer, S. König, and U. van Kolck, "Nuclear effective field theory: Status and perspectives," Rev. Mod. Phys. **92**, 025004 (2020), DOI: 10.1103/RevModPhys.92.025004.

[43] T. Otsuka, A. Gade, O. Sorlin, T. Suzuki, and Y. Utsuno, "Evolution of shell structure in exotic nuclei," Rev. Mod. Phys. **92**, 015002 (2020), DOI: 10.1103/RevModPhys.92.015002.

[44] H. Hergert, S. K. Bogner, T. D. Morris, A. Schwenk, and K. Tsukiyama, "The in-medium similarity renormalization group: A novel ab initio method for nuclei," Phys. Rep. **621**, 165 (2016), DOI: 10.1016/j.physrep.2015.12.007.

[45] J. M. Lattimer and M. Prakash, "The equation of state of hot, dense matter and neutron stars," Phys. Rep. **621**, 127 (2016), DOI: 10.1016/j.physrep.2015.12.005.

[46] J. M. Lattimer, "Neutron stars and the nuclear matter equation of state," Annu. Rev. Nucl. Part. Sci. **71**, 433 (2021), DOI: 10.1146/annurev-nucl-102419-124827.

[47] B. P. Abbott *et al.* (LIGO Scientific Collaboration and Virgo Collaboration), "GW170817: Observation of gravitational waves from a binary neutron star inspiral," Phys. Rev. Lett. **119**, 161101 (2017), DOI: 10.1103/PhysRevLett.119.161101.

[48] M. J. Dolinski, A. W. P. Poon, and W. Rodejohann, “Neutrinoless double-beta decay: Status and prospects,” Annu. Rev. Nucl. Part. Sci. **69**, 219 (2019), DOI: 10.1146/annurev-nucl-101918-023407.

[49] M. Agostini, G. Benato, J. A. Detwiler, J. Menéndez, and F. Vissani, “Toward the discovery of matter creation with neutrinoless $\beta\beta$ decay,” Rev. Mod. Phys. **95**, 025002 (2023), DOI: 10.1103/RevModPhys.95.025002.

[50] P. Gysbers *et al.*, “Discrepancy between experimental and theoretical β-decay rates resolved from first principles,” Nature Phys. **15**, 428 (2019), DOI: 10.1038/s41567-019-0450-7.

[51] H. L. Crawford, K. Fossez, S. König, and A. Spyrou, “A vision for the science of rare isotopes,” Annu. Rev. Nucl. Part. Sci. **74**, 141 (2024), DOI: 10.1146/annurev-nucl-121423-091501.

[52] Nuclear Science Advisory Committee, *A New Era of Discovery: The 2023 Long Range Plan for Nuclear Science*, U.S. Department of Energy and National Science Foundation (2023), `https://nuclearsciencefuture.org/`.

[53] S. A. Giuliani, Z. Matheson, W. Nazarewicz, E. Olsen, P.-G. Reinhard, J. Sadhukhan, B. Schuetrumpf, N. Schunck, and P. Schwerdtfeger, “Colloquium: Superheavy elements: Oganesson and beyond,” Rev. Mod. Phys. **91**, 011001 (2019), DOI: 10.1103/RevModPhys.91.011001.

[54] N. Schunck and D. Regnier, “Theory of nuclear fission,” Prog. Part. Nucl. Phys. **125**, 103963 (2022), DOI: 10.1016/j.ppnp.2022.103963.

[55] I. Counts, J. Hur, D. P. L. Aude Craik, H. Jeon, C. Leung, J. C. Berengut, A. Geddes, A. Kawasaki, W. Jhe, and V. Vuletić, “Evidence for nonlinear isotope shift in Yb^+ search for new boson,” Phys. Rev. Lett. **125**, 123002 (2020), DOI: 10.1103/PhysRevLett.125.123002.

[56] I. Angeli and K. P. Marinova, “Table of experimental nuclear ground state charge radii: An update,” At. Data Nucl. Data Tables **99**, 69 (2013), DOI: 10.1016/j.adt.2011.12.006.

[57] S. Kraemer *et al.*, “Observation of the radiative decay of the ^{229}Th nuclear clock isomer,” Nature **617**, 706 (2023), DOI: 10.1038/s41586-023-05894-z.